Journal of Applied Geophysics 208 (2023) 104869

Contents lists available at ScienceDirect

Journal of Applied Geophysics

journal homepage: www.elsevier.com/locate/jappgeo

Probabilistic inversion of audio-frequency magnetotelluric data and application to cover thickness estimation for mineral exploration in Australia

Wenping Jiang *, Ross C. Brodie, Jingming Duan, Ian Roach, Neil Symington, Anandaroop Ray, James Goodwin

Geoscience Australia, GPO Box 378, Canberra, ACT 2601, Australia

A B S T R A C T

We have applied a Bayesian inference algorithm and released open-source code for the 1D inversion of audio-frequency magnetotelluric data. The algorithm uses a trans-dimensional Markov chain Monte Carlo technique to solve for a probabilistic resistivity-depth model. The inversion employs multiple Markov chains to generate an ensemble of millions of resistivity models that adequately fit the data given the assigned noise levels. The trans-dimensional aspect of the inversion means that the number of layers in the resistivity model is solved for rather than being predetermined. The inversion scheme favours a parsimonious solution and the acceptance criterion ratio is theoretically derived such that the Markov chain will eventually converge to an ensemble that is a good approximation of the posterior probability density (PPD). Once the ensemble of models is generated, its statistics are analysed to assess the PPD and to quantify model uncertainties. This approach gives a thorough exploration of model space and a more robust estimation of uncertainty than deterministic methods allow.

We demonstrate the application of the method to cover thickness estimation for a number of regional drilling programs. Comparison with borehole results demonstrates that the method is capable of identifying major stratigraphic units with resistivity contrasts. Our results have assisted with drill site targeting and have helped to reduce the uncertainty and risk associated with intersecting targeted stratigraphic units in covered terrains. Interpretation of the audio-frequency magnetotelluric data has improved our understanding of the distribution and geometries of sedimentary basins. From an exploration perspective, mapping sedimentary basins and covered near-surface geological features supports the effective search for mineral deposits in greenfield areas.

1. Introduction

The electrical conductivity of Earth materials is sensitive to temperature, fluid content and geochemical constituents, e.g. metallic sulphides and graphite (e.g. Ferguson et al., 1999); therefore, mapping conductivity variations in Earth materials is useful for mineral, geothermal, and hydrocarbon exploration, as well as groundwater detection and monitoring. Magnetotellurics (MT) measures the natural magnetic and electric fields of the Earth, caused by the interaction of the solar wind and magnetosphere at low frequencies (< 1 Hz) and by global lightning activity at high frequencies (> 1 Hz). The MT technique (Cagniard, 1953; Tikhonov, 1950), along with appropriate data inversion and interpretation, provides a means to investigate conductivity distribution in the subsurface from a few tens of meters to hundreds of kilometres depth, depending on the frequencies of the measurement. Audio-frequency magnetotellurics (AMT) samples signals in the frequency range of ~1 Hz to 10 kHz, pertaining to a few kilometres in the upper crust, and is applicable to shallow resource exploration.

Conventional methods for geophysical inversion usually utilise gradient-based deterministic optimisation techniques; for example, Gauss-Newton methods (Pratt et al., 1998), steepest descent techniques (Roy, 2002), and conjugate gradients methods (Newman and Alumbaugh, 2000; Rodi and Mackie, 2001; Siripunvaraporn and Egbert, 2007). Typically, these methods strive to minimise an objective function comprising data misfit and model regularisation terms (e.g., Constable et al., 1987). The final solution is a single model that fits the data within the assigned noise levels and conforms as closely as possible to the constraints imposed by some form of regularisation. The solution often depends on a combination of the initial parameters and regularisation. As Brodie and Sambridge (2012) point out, the single model is just one of an infinite suite of models that could possibly fit the data within the noise levels. On its own, the single solution provides no information about the non-uniqueness or uncertainty in the solution. Some methods make use of the posterior model covariance matrix to estimate model parameter uncertainties. However, strictly speaking, such estimates are accurate only for linear problems and they cannot take account of the

* Corresponding author.
E-mail address: wenping.jiang@ga.gov.au (W. Jiang).

https://doi.org/10.1016/j.jappgeo.2022.104869
Received 4 January 2022; Received in revised form 11 August 2022; Accepted 7 November 2022
Available online 11 November 2022

non-linearity or non-uniqueness of the electromagnetic inverse problem.

Probabilistic inversion methods have been recognised as a powerful approach to addressing the non-uniqueness problem and quantifying uncertainty. A probabilistic method does not settle on one best model but samples millions of models that all fit the data given the assigned noise levels. The inversion results are driven by data and prior assumptions and are independent of initial parameters and regularisation. Probabilistic methods do not rely on linearisation and, therefore, are able to deal with strong nonlinearity (Dettmer and Dosso, 2013). Bayes' Theorem (Bayes and Price, 1763) has been successfully applied to a broad range of applications and Markov chain Monte Carlo (McMC) algorithms have primarily been used to draw samples. Within a Bayesian framework, a probabilistic model of the parameter objective function is built based on a direct search of the global space, and the solution provided is a (posterior) probability distribution (PPD). Model uncertainty can be quantified by assessing the PPD of the model parameters.

In the last decade, the trans-dimensional (often called reversible jump) Markov chain Monte Carlo (rj-McMC) method has gained increasing traction in geophysics since it was first introduced by Green (1995). The trans-dimensional aspect of the algorithm allows model parameter to be solved for and model complexity to be inferred from the data. It has been applied to seismic tomography and receiver function data (Bodin and Sambridge, 2009; Bodin et al., 2012), airborne electromagnetics data (Brodie and Sambridge, 2012; Minsley, 2011), and marine controlled source electromagnetic data (Ray and Key, 2012). More recently, it has been implemented in the 1D inversion of magnetotelluric (MT) data (Mandolesi et al., 2018; Peng et al., 2022; Xiang et al., 2018) and joint inversion of controlled source electromagnetic and MT data (Blatter et al., 2019). Blatter et al. (2021), for the first time, applied a 2D trans-dimensional Markov chain Monte Carlo algorithm to invert MT data by using a Gaussian process (GP) to achieve a parsimonious model representation and, by utilising high performance computing infrastructure, to efficiently sample the model space. While these studies provided detailed algorithm development and statistical exploration of model parameters, few of them sufficiently demonstrated the application and validation of the method using real data.

We present our implementation of a Bayesian inference reversible jump Markov chain Monte Carlo method to perform 1D inversion of AMT data for near-surface exploration. The method is similar to that proposed by Mandolesi et al. (2018), with differences in the recipe for proposing a candidate model. Tests of the method on synthetic data were reported in Brodie and Jiang (2018). In real cases, we have applied the method to estimate depth to basement in sedimentary basins, and validated its application by comparing with other observations including refraction seismic, airborne magnetic data and drill results. For example, we have successfully applied the method to cover thickness estimation for a number of regional drilling programs across Australia (Figure 1) which, in turn, provide ground-truth borehole results to test the models. Here we report outcomes from inversion of AMT data to characterise cover and discuss the implications for mineral exploration.

2. MT Theory

The MT technique makes use of simultaneous measurements of the Earth's magnetic and electric fields as an electromagnetic induction source to derive resistivity structure in the subsurface (Cagniard, 1953; Tikhonov, 1950). The basis of the MT technique is that the penetration depth of electromagnetic waves depends on the sounding frequency/period and on the resistivity structure of the subsurface. Based on the assumption that the primary electromagnetic field is a plane wave impinging on the Earth with vertical incidence and travelling in a diffusive manner within the Earth, the propagation of electromagnetic fields through the Earth materials can be mathematically solved using Maxwell's equations by applying the boundary conditions across discontinuities (layers interfaces) (Dmitriev and Berdichevsky, 1979; Vozoff, 1991). The complex ratios of the orthogonal components of

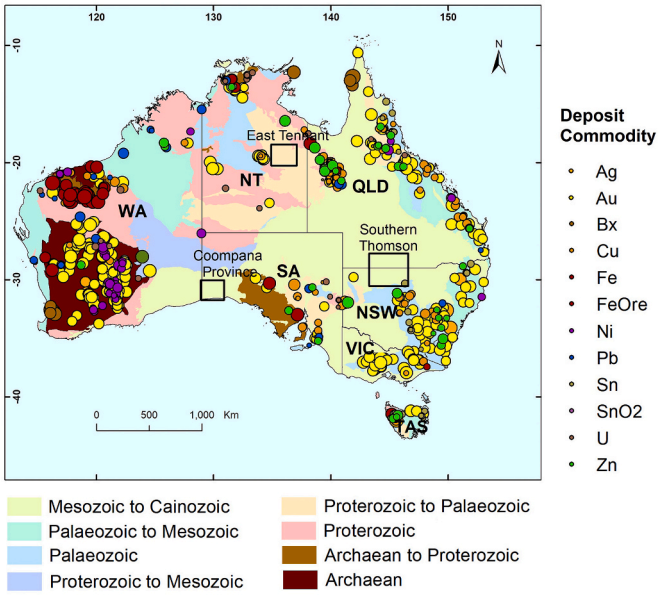

Fig. 1. Location of the three recently completed regional drilling programs in Southern Thomson, Coompana Province, and East Tennant, overlain on the Geological Regions of Australia map, 1:5 000 000 scale (Blake et al., 2012). Data source of deposit commodity: OzMin database

magnetic (H) and electric (E) fields, expressed as an impedance tensor (Z), are used to describe the penetration of electromagnetic fields into the Earth (Cagniard, 1953; Tikhonov, 1950; Ward and Hohmann, 1988). The impedance tensor and the electric and magnetic fields are related as:

$$\begin{bmatrix} E_x \\ E_y \\ H_z \end{bmatrix} = \begin{bmatrix} Z_{xx} & Z_{xy} \\ Z_{yx} & Z_{yy} \\ T_{xz} & T_{yz} \end{bmatrix} \begin{bmatrix} H_x \\ H_y \end{bmatrix} \tag{1}$$

The amplitude of the impedance tensor Z is commonly expressed in terms of apparent resistivity through the relation:

$$\rho_a(\omega) = \frac{1}{\omega\mu_0}\left|\frac{E_x}{H_y}\right|^2 = 0.2T\left|\frac{E_x}{B_y}\right|^2 \tag{2}$$

and phase angle indicating the phase shift between the electrical and magnetic field components:

$$\phi_a(\omega) = tan^{-1}\frac{imag\left[\frac{E_x}{H_y}\right]}{real\left[\frac{E_x}{H_y}\right]} \tag{3}$$

where $\rho_a(\omega)$ is the apparent resistivity in ohm.m at angular frequency ω, $\varnothing$ is the phase angle in degrees, T is the period (reciprocal of the frequency) and μ_0 is the magnetic permeability value in a vacuum. When collecting field data, the electric field E is measured in mV/km and the magnetic field is measured as magnetic induction B in nT, instead of the magnetic intensity H, where $B = \mu_0 H$.

MT responses are sensitive to the dimensionality and direction of the structure beneath, and such information is reflected in the impedance tensor. For a layer-cake 1D Earth, where conductivity only varies with depth, the diagonal elements of the impedance tensor, Z_{xx} and Z_{yy} (which couple parallel electric and magnetic field components), are zero while the off-diagonal components (which couple orthogonal electric and magnetic field components), Z_{xy} and Z_{yx}, are equal in magnitude but have opposite signs. For a 2D Earth, where conductivity varies with depth and along one direction, the diagonal elements of the impedance tensor are zero, while the off-diagonal components are different. The direction in which the conductivity of a 2D structure does not vary is termed the strike (principal conductivity axis). If the impedance is

measured at an arbitrary orientation, the measurements need to be rotated into a 2D form or a best-fitting 2D form during 2D analysis (Booker, 2014; Caldwell et al., 2004). For a 3D Earth, conductivity varies in all directions and the four impedance tensor components are individually different.

In a layered 1D Earth, in which each layer has constant resistivity and thickness, the impedance tensor can be solved from the bottom uniform half-space (bottom layer of the model) and computed iteratively to the topmost layer by applying boundary conditions that transmit and reflect electromagnetic waves (Kaufman and Keller, 1981).

The rotational invariants of the impedance tensor Z are independent of the direction of the inducing field and measurement orientations (Szarka and Menvielle, 1997) and, therefore, are useful for MT analysis. Among a number of rotational invariants, the difference between off-diagonal elements,

$$Z_1 = \left(Z_{xy} - Z_{yx}\right)/2 \tag{4}$$

the sum of the diagonal elements (known as the trace),

$$Z_2 = \left(Z_{xx} + Z_{yy}\right)/2 \tag{5}$$

and the determinant of the impedance,

$$det(Z) = \sqrt{\left|Z_{xx}Z_{yy} - Z_{xy}Z_{yx}\right|} \tag{6}$$

are often used for data inversion and interpretations.In addition, the geometric mean of the apparent resistivity $\sqrt{\rho_{xy}\rho_{yx}}$ and the arithmetic mean of the apparent phase $((\theta_{xy} + \theta_{yx})/2)$ are often used for 1D modelling, although the off-diagonal components are supposed to be equal in a perfect 1D structure

3. Bayesian Inference via a rj-McMC Algorithm

We have developed a computer program, which we call *rj-McMCMT*, to perform 1D inversion of AMT data in a Bayesian framework using reversible jump Markov chain Monte Carlo sampling. The source code and user document can be downloaded from Geoscience Australia's GitHub® repository https://github.com/GeoscienceAustralia/rjmcmcmt. It is built upon an open-source *rj-McMC* library (Hawkins, 2013; Sambridge et al., 2013) developed at the Research School of Earth Sciences, Australian National University (http://www.iearth.org.au/codes/rj-MCMC/). The library provides low-level routines for running reversible jump Monte-Carlo Markov chains for 1D and 2D spatial regression problems and also allows generalisation to any spatial 1D and 2D problem through a user-supplied data misfit function. For more details about the library, interested readers are referred to Denison et al. (2002), Gallagher et al. (2011), Sambridge et al. (2013) and Hawkins (2013). Specifically, our program makes use of the 1D inversion functionality in the *rj-McMC* library through the function *MPI_part1d_forwardmodel*.

Our program calls *MPI_part1d_forwardmodel* to perform the trans-dimensional sampling and, in doing so, it passes our routine that is called when every proposed 1D resistivity model is sampled. Our routine calculates the 1D MT forward response of the proposed model and returns the negative-log-likelihood (0.5 × chi-squared and log-value of the normalising factor) of the model given the observed data and assigned noise levels. The proposed new model may or may not be accepted and added onto the end of the Markov chain. If the proposed model is not accepted a copy of the current model is added to the end of the chain. The trans-dimensional aspect of the algorithm allows the number of layers in the resistivity model to be a parameter to be solved for in the inversion itself, meaning the number of layers does not need to be fixed in advance.

Our forward modelling routine generates the MT data for an isotropic layered resistivity model at the specific list of frequencies for which the observed data are available. The program has options to invert data in the form of either real and imaginary impedance or apparent resistivity and phase, directly from field data in a standard Electrical Data Interchange (EDI) format. When inverting impedance data we use the determinant of the impedance tensor (Equation (6)). When inverting apparent resistivity and phase data, we use the geometric mean of the apparent resistivity and the arithmetic mean of the apparent phase. Relative and absolute noise standard deviation estimates for the data are specified and combined (assuming independence) to generate the total noise estimate that is used in the inversion to calculate the noise-normalised (*L2-norm)* data misfit (chi-squared).

Figure 2 describes the probabilistic inversion workflow. The program is parallelised using the Message Passing Interface (MPI) paradigm. For each AMT station, multiple Markov chains are executed in parallel on a cluster computer or multi-core workstation. Each chain is initialised with a model randomly drawn from the prior probability distribution.

The algorithm assumes uniform prior probability for the number of layers in the model and a log-uniform prior on the depths of the layer interfaces. The latter is because depth in the model is parameterised in terms of logarithmic depth. As the chain samples new models the algorithm is allowed to make one of four types of perturbations to the current model: (a) change to the resistivity of a layer (*value change*); (b) move an interface up or down (*interface move*); (c) create a new interface (*birth*); or (d) remove an interface (*death*). The new model is proposed by drawing random perturbations from a Gaussian proposal distribution. The proposed model is either accepted or rejected based on an acceptance criterion ratio. The acceptance criterion ratio is theoretically derived such that the Markov chain will eventually converge to an ensemble that is a good approximation of the PPD of the model given the data and supplied noise estimates. Details of the derivation of the acceptance ratio are given in Bodin et al. (2012). For the value-change and interface-move propositions, the sampling algorithm favours accepting models with higher likelihoods (lower data misfits) and higher prior likelihoods than the current model. For the birth and death

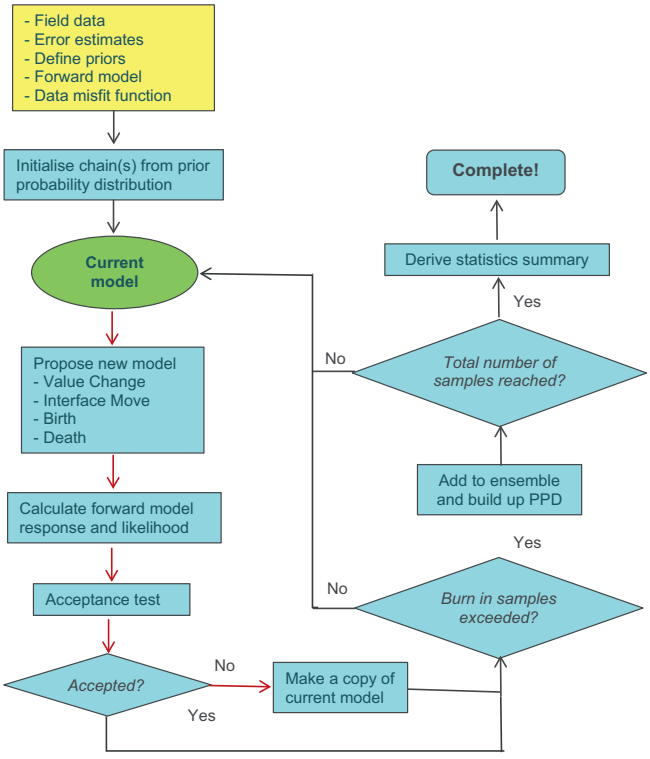

Fig. 2. Probabilistic sampling workflow using the rj-McMCMT algorithm to perform 1D inversion of audio magnetotellurics (AMT) data.

propositions, the acceptance probability is a balance between the proposal probability, which encourages resistivity changes between adjacent layers, and the difference in data misfit, which penalises changes if they degrade the data fit. Also, given similar data fits, a proposed model has more chance of being accepted if it has fewer layers than the current model. This gives the algorithm a form of natural parsimony (Bodin and Sambridge, 2009; Malinverno, 2002) by adapting Occam's minimum structure philosophy (Constable et al., 1987). It is implemented by using the Occam Factor as the ratio of posterior accessible volume to prior accessible volume to penalise more complex parametrisations (MacKay, 2003; Ray et al., 2016).

The number of samples (models) for the burn-in period of the Markov chain is specified by the user, which allows the data misfit to converge to an acceptable level before any samples are accepted into the ensemble. The convergence history from a test run can give an indication of the number of samples needed for the burn-in period. After the burn-in period, new models are added into a discretised 2D PPD histogram. That is, for each discrete histogram depth-bin, the model resistivity is determined and the corresponding histogram resistivity-bin count is incremented. This progressively builds up an image representation of the desired posterior probability. Similarly, a 1D change-point histogram is built up by incrementing all depth-bins of the 1D histogram in which a layer interface falls. At the conclusion of the sampling the PPD and the change-point histograms from all the parallel chains are merged. The single most probable (highest likelihood) and lowest misfit models from all chains are also saved. An example is given in Figure 3.

Statistics summaries can be derived to assess the PPD of resistivity at depth and to quantify the model uncertainty. One of the measures for quantifying model uncertainty is a credible interval delineated by percentiles of the posterior distribution. A larger credible interval indicates a higher degree of variability in the models (samples) and suggests a higher uncertainty. Another measure of uncertainty is to use the 1D change-point histogram, which describes the probability of a resistivity layer interface occurring at a particular depth bin. This histogram can be interrogated to assess the probability of a peak falling at a particular depth and in some cases can be used to quantify layer boundary uncertainty. In this study, the full width at half maximum (FWHM) statistic is used to estimate the uncertainty of a layer boundary interface. The FWHM is calculated by finding the width in metres of the peak at half of its maximum probability, where the larger the FWHM value the higher uncertainty of the depth estimate.

4. Applications and Results

Approximately 80% of Australia is covered by sedimentary basins and regolith and is largely under-explored. To improve understanding of cover sequences, basement geology and mineral potential, Geoscience Australia has undertaken a number of regional stratigraphic drilling programs in covered terrains in collaboration with Australian state and territory geological surveys. We have applied the *rj-McMCMT* method to estimate cover thickness from AMT data for drilling programs in the Southern Thomson, Coompana Province and East Tennant regions of Australia (Figure 1).

4.1. Southern Thomson

The Southern Thomson drilling program is in the Paleozoic Thomson Orogen region of southern Queensland and northern New South Wales

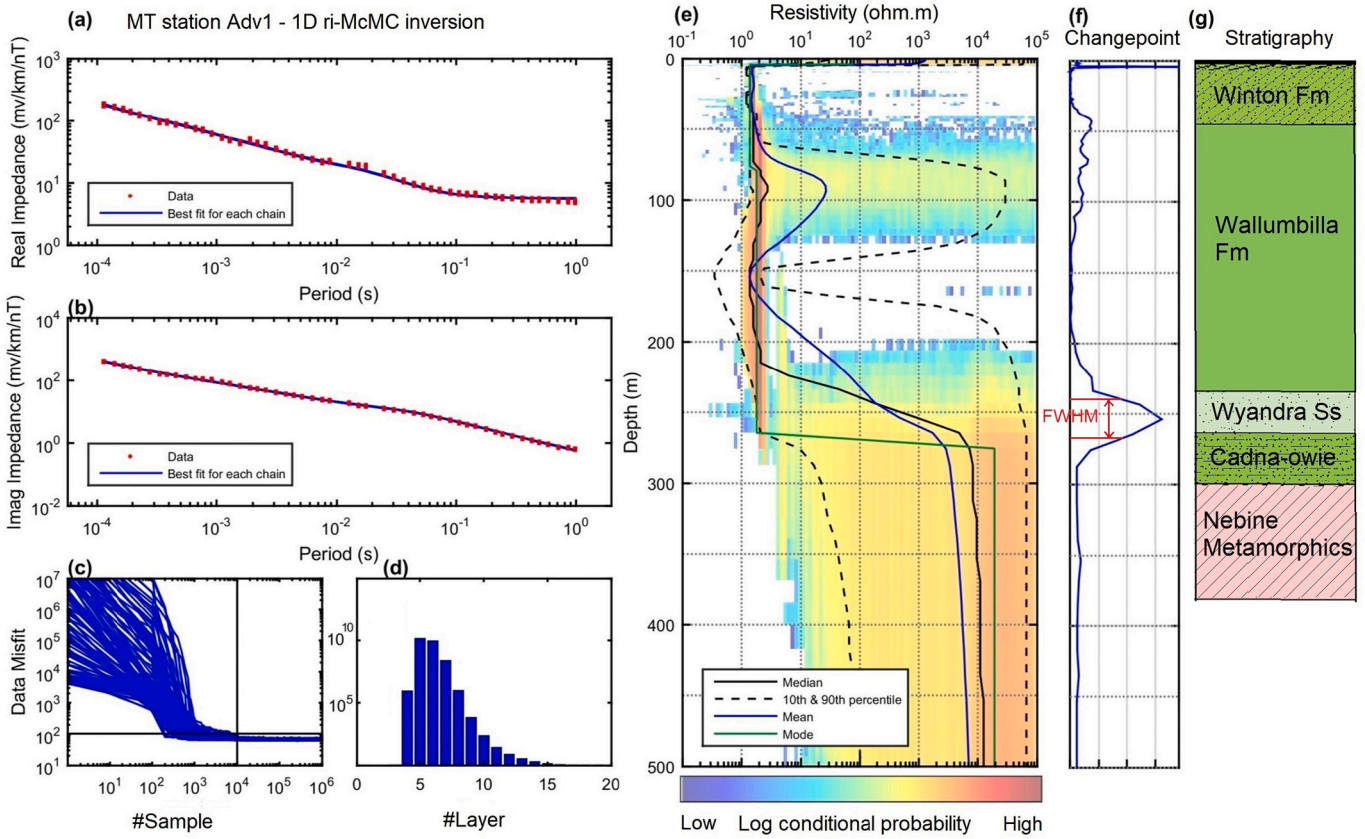

Fig. 3. Plot summarising the results of the rj-McMCMT inversion at Site GSQ Eulo 1 (Roach et al., 2017): (a) & (b) real and imaginary impedances and error bars (red) and the best fitting model from each Markov chain (blue); (c) data misfit convergence history for each Markov chain (10^4 burn-in period); (d) histogram of the number of model layers; (e) the summary median, 10^{th} and 90^{th} percentile, mean and mode models overlying the pseudo-coloured shaded image of the 2D log-PPD histogram; (f) the change-point histogram showing the probability of where layer interfaces occur and FWHM quantifying the uncertainty; and (g) the stratigraphic log from the adjacent borehole.

(Figure 1). It is largely concealed by Mesozoic sedimentary rocks of the Eromanga Basin and younger sedimentary rocks. Basement rocks of the Thomson Orogen are identified to have potential to host gold and intrusion-related Mo-W mineral systems (Armistead et al., 2017; Rothery, 2013).

We used AMT, refraction seismic and airborne magnetic data to estimate cover thickness at proposed drill sites in the southern Thomson Orogen as part of the pre-drilling geophysics campaign in 2016, which aimed to reduce the uncertainty and risk associated with intersecting the targeted stratigraphy. We inverted AMT data (Jiang, 2017) at each site using 128 Markov chains with each chain sampling 1 million models. We then interpreted the posterior ensemble results and estimated cover thickness using the resistivity contrast between the overlying Eromanga Basin and the basement. Comparison with drillhole results indicates that the method is capable of identifying major stratigraphic structures and providing cover thickness estimates with a reasonable accuracy.

We selected the drill site GSQ Eulo 1 (MT station Adv1) as an example. We inverted the impedance tensor determinant for 40 frequencies in the range 1 Hz to 10 kHz. For both real and imaginary components we assessed the data errors to be 5% relative noise and 0.025 mV/km/nT noise floor. We specified the maximum depth of the layer interfaces to be two times the maximum skin depth to allow electromagnetic waves to decay. The maximum number of layers allowed in the resistivity model was set at 20. The minimum and maximum resistivity range (0.1 to 100,000 Ωm) is specified in $\log_{10}$ units. A summary of the results is given in Figure 3.

Figure 3a and 3b show real and imaginary components of the impedance tensor with their assigned error bars, and the predicted data from the best-fitting model for each of the 128 Markov chains, which happen to plot almost exactly on top of one another and fit the observation data reasonably well. The number of samples (models) for the burn-in period is specified as 10,000, which allows the models to converge before any samples are accepted into the ensemble. Because data misfit is normalised by data error, an ideal value of 1 is an indication of model convergence. For a visualisation purpose, in Figure 3c we plot twice that of the total data misfit. As demonstrated by the convergence history, after the burn-in period, the chains are converging from high data misfits down to the expected data misfit of 80 (i.e., twice of the total number of data) represented by the horizontal line. After the burn-in the chains remain fitting the data at close to the expected value. Figure 3d indicates that a 5 or 6-layer model is the most likely.

Several statistics are extracted from the 2D log-PPD histograms including the mean, mode, 10^{th}, 50^{th} (median) and 90^{th} percentile log-resistivity values in each depth-bin (Figure 3e). These suggest a high posterior probability for a very conductive zone in the top 50 m that corresponds well with the weathered Winton Formation (0-48 m) of the Eromanga Basin as shown on the stratigraphy log (Figure 3g). The borehole lithology shows yellow goethite and reddish hematite patches with iron concretions (Roach et al., 2017), which would contribute to high conductivities. The inversion results suggest the remainder of the Eromanga Basin sequence is predominantly conductive, with some possibility of resistive zones, until approximately 250 m where a significant transition from conductive to resistive material occurs. The broad peak of the transition in the change-point histogram between 225-275 m coincides with the Wyandra Sandstone Member or Cadna-owie Formation. Because these formations have similar electrical resistivity properties, the MT responses cannot distinguish them due to weak resistivity contrasts. Below 275 m the inversion profile is definitively resistive, representing a basement consisting of Nebine Metamorphics greenschist (part of the Thomson Orogen).

We also compared cover thickness estimates from AMT, refraction seismic and airborne magnetic data with borehole results at three actually drilled sites (Figure 4; (Goodwin et al., 2018)). The AMT method provided cover thickness estimates that are in reasonable agreement with drilled basement depths at all three sites. This is because the Eromanga Basin sediments form a conductive cover that can readily be distinguished from the resistive basement geology.

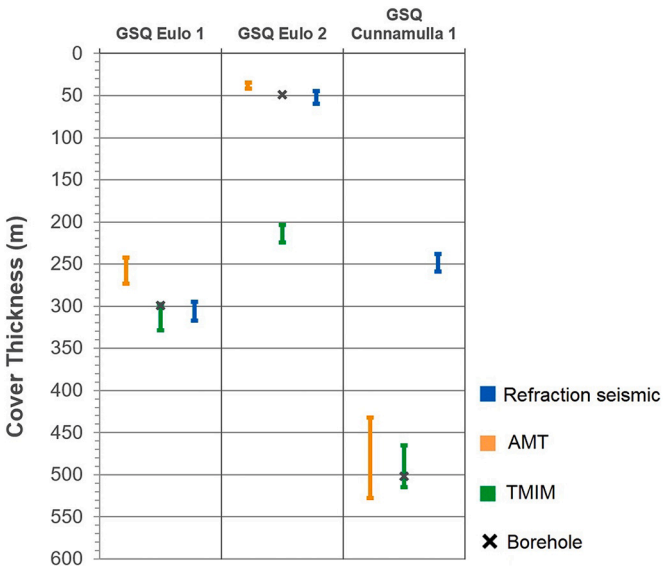

Fig. 4. Comparison of cover thickness estimates with uncertainty from AMT, refraction seismic and airborne magnetic data with borehole results at three drill sites (Goodwin et al., 2017; Goodwin et al., 2018).

Cover thickness estimates from airborne magnetic data using a Targeted Magnetic Inversion Modelling (TMIM) method (Goodwin et al., 2017) were able to predict the basement depth in two out of three cases. However, this technique suffers from the fact that a suitable magnetic source anomaly is required in the area of interest, and this was not always the case at these sites. This issue is highlighted at GSQ Eulo 2, where the borehole was located on an isolated and steep-sided basement high (Roach et al., 2015) and the depth to basement is shallow (51 m). However, the magnetic anomaly was sourced from a target adjacent to (and deeper than) the borehole target that resulted in an overestimation of the cover thickness.

At a deeper site (GSQ Cunnamulla 1), seismic refraction underestimated the depth to basement, because the resolvable depth by the refraction seismic method was limited to ~300 m by the seismic source. Note that the depth ranges inferred from seismic refraction represent the topographic variations along a 2D layer that was modelled, rather than actual uncertainties as in the other methods.

Interpretation using various independent geophysical methods provides more information about the nature of the basement-cover interface throughout the southern Thomson Orogen. In particular, that it is weathered, it has mappable topography, and it can be recognised by its seismic velocity, electrical conductivity and magnetic susceptibility contrasts. As no one technique provided perfect predictions of cover thickness in all situations, it is recommended that several geophysical techniques be used as complementary methods to determine cover thickness in greenfield terrains.

4.2. *Coompana province*

The Coompana Province straddles the South Australian–Western Australian border in South Australia's far west (Figure 1). It is completely covered by Neoproterozoic to Cenozoic sediments of the Officer, Denman, Bight and Eucla basins, and there are no known records of outcropping basement. The geology of the Province is poorly understood and the mineral prospectivity of the South Australian part of the Province is largely unknown.

The Coompana Drilling Project was a collaborative project between Geoscience Australia and the Geological Survey of South Australia, co-funded by Geoscience Australia's Exploring for the Future program

and the South Australian Government's PACE Copper initiative. As part of the pre-drilling geophysics program, we applied the MT method to estimate cover thickness for drill targeting. We collected MT data at six historic boreholes in 2016 and at eight proposed drill sites in 2017 (Jiang et al., 2017). One and two-dimensional modelling were undertaken using different methods to improve confidence levels, which included the non-linear conjugate gradient (NLCG) algorithm of Rodi and Mackie (2001, 2012), Occam's inversion (Constable et al., 1987) and the trans-dimensional Markov chain Monte Carlo algorithm. An example of model results and comparison with drill result at borehole CDP003 are given in Figure 5 and Figure 6.

Model results show the presence of a moderately resistive layer in the upper few tens of metres (~50 m), which is interpreted as the Nullarbor Limestone. Beneath, it is evident that the MT responses transitioned from resistive to conductive rocks, from chalky fossiliferous limestone (Wilsons Bluff Limestone) to a more conductive structure which is characterised by resistivities less than 10 Ωm. This layer (~120 to ~250 m) is interpreted as Pidinga Formation and/or Madura Formation, likely to be unconsolidated deposits, e.g. claystone/siltstone with shale, or carbonaceous mudstone/sandstone. The enhanced conductivity may also be attributed to sediments or rocks saturated with groundwater. Because these formations have similar electrical conductivity properties, the MT responses cannot distinguish them due to weak conductivity contrasts. The diffusive nature of electromagnetic techniques also smears sharp boundaries and thin layers (Constable et al., 1987). At greater depths (>~250 m), the resistivity value gradually increases from 10 Ωm to 10^2-10^3 Ωm, representing the Loongana Formation (sandstone) and the underlying basement (Moodini Supersuite).

The cover thickness estimates at five boreholes compare favourably (Figure 7) with drilling results with a variable accuracy of 0.5% to 14%.

4.3. East Tennant project

The East Tennant project area is located east of the Tennant Creek district in the Northern Territory (Figure 1), and is defined by an approximately northeast-trending corridor extending to the Queensland border. The Proterozoic Warramunga Province, exposed in the vicinity of Tennant Creek, hosts iron-oxide-copper gold mineralisation. The East Tennant area is almost completely covered by sedimentary rocks of the Georgina Basin and Kalkarindji Igneous Province, whereas the extent of the Paleo-Mesoproterozoic South Nicholson Basin has not been mapped precisely due to limited and sparsely distributed boreholes. Despite the lack of exposed basement rocks in the area, this under-explored region is considered to have significant mineral potential (Czarnota et al., 2020; Murr et al., 2020; Schofield et al., 2020; Skirrow et al., 2019).

Geoscience Australia, in partnership with the MinEx CRC and Northern Territory Geological Survey, undertook a drilling campaign in the East Tennant region during late 2020 as part of the National Drilling Initiative (NDI). Prior to drilling, geophysical surveys were conducted to acquire higher-resolution gravity and MT data in the East Tennant

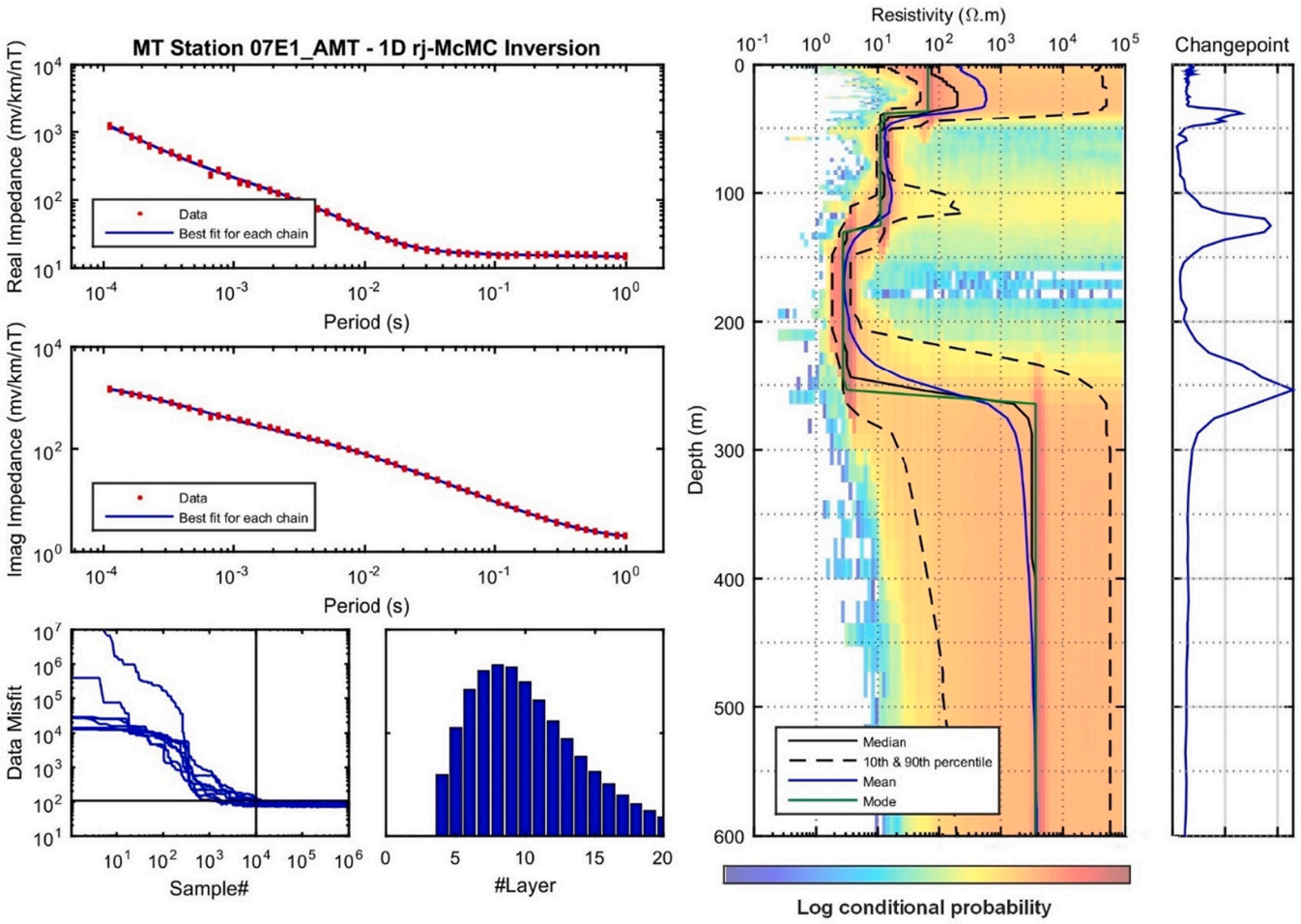

Fig. 5. Plot summarising the results of the rj-McMCMT inversion at MT site 07E1 near borehole CDP003: (a) & (b) real and imaginary impedances and error bars (red) and the best fitting model from each Markov chain (blue); (c) data misfit convergence history for each Markov chain (10^4 burn-in period); (d) histogram of the number of model layers; (e) the summary median, 10th and 90th percentile, mean and mode models overlying the pseudo-coloured shaded image of the 2D log-PPD histogram; (f) the change-point histogram showing the probability of where layer interfaces occur.

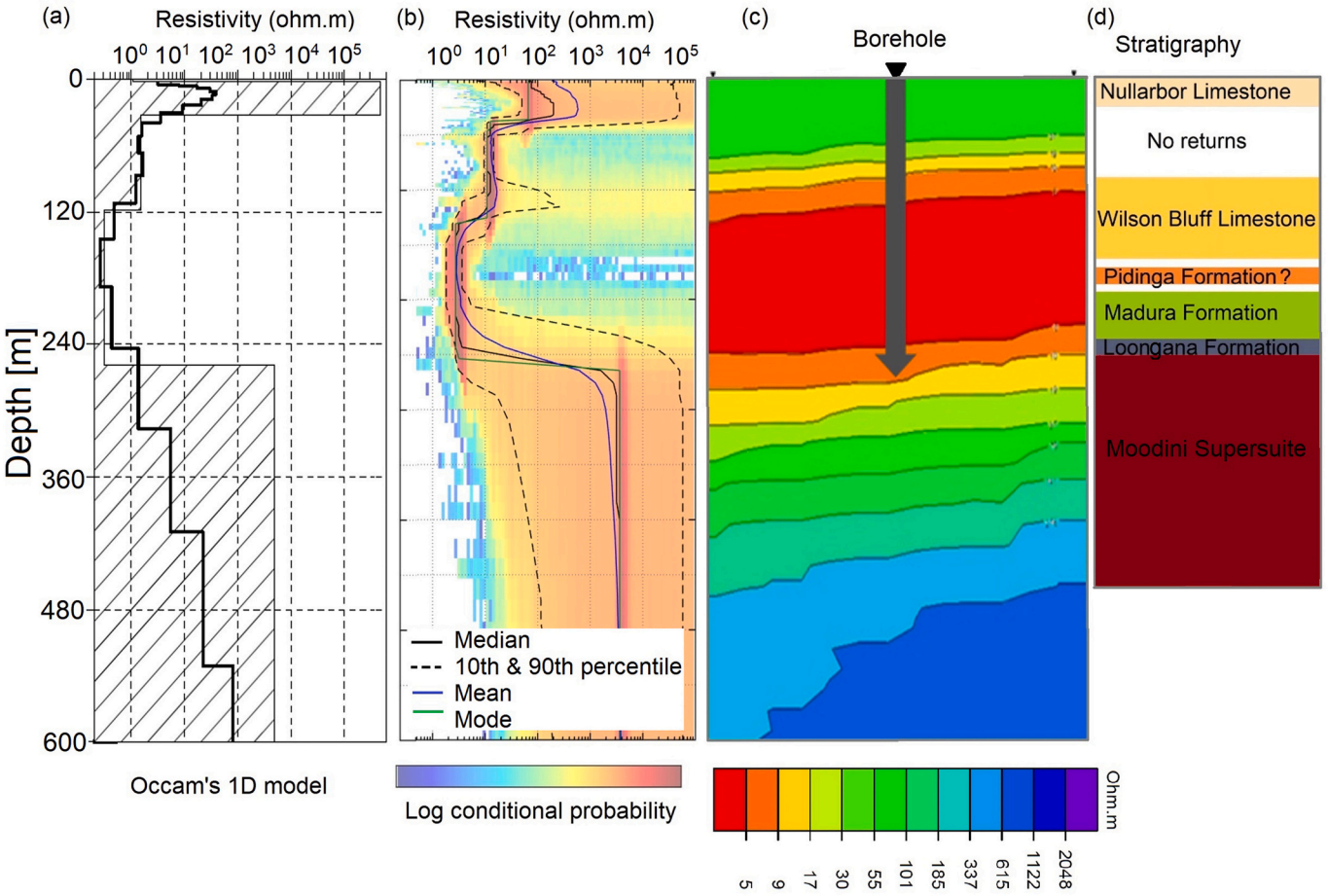

Fig. 6. MT model results near borehole CDP003: (a) 1D resistivity model from Occam's inversion (black line showing the Occam model and hatched blocks showing the estimated resistivity structure); (b) 2D log-PPD histogram with pseudo-coloured shading and the summary models from rj-McMCMT; (c) model section from the 2D non-linear conjugate gradient (NLCG) algorithm; (d) stratigraphy log at borehole CDP003 (Dutch et al., 2017).

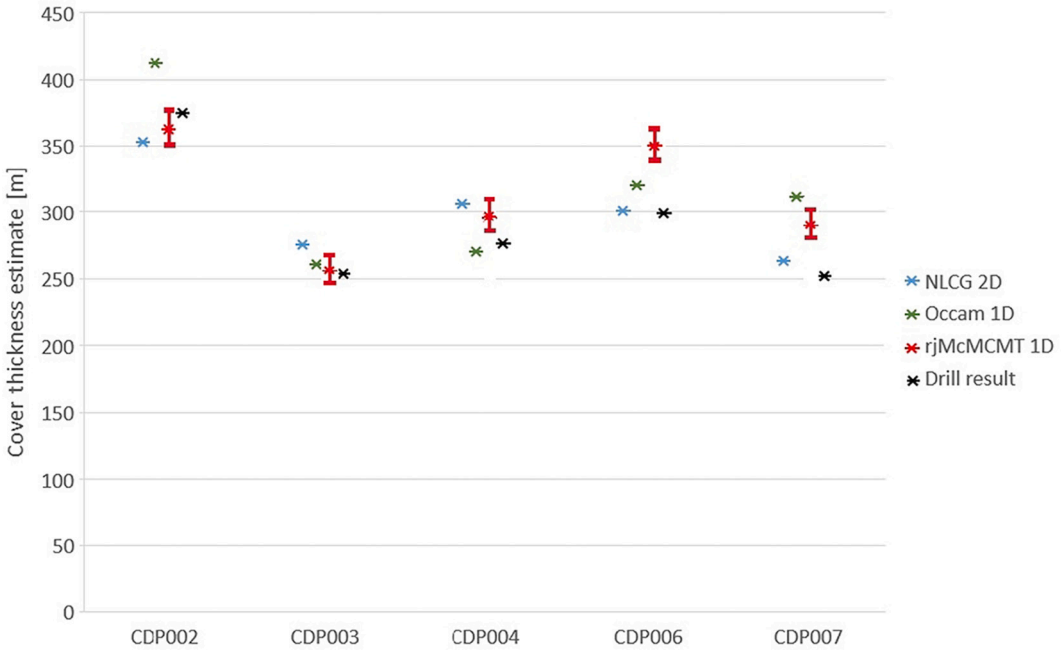

Fig. 7. Cover thickness estimates from the Occam 1D, NLCG 2D and rj-McMCMT 1D inversion results compared to the drilling results (true vertical depth). The rjMcMCMT 1D results are interpreted from the change point peaks at the depth of transition from the conductive sedimentary basins to the resistive basement, and are presented with the FWHM uncertainty of the peak distribution.

region (Jiang and Duan, 2019). In July and August 2019, broadband MT and AMT data were acquired at 131 stations including ten proposed drill sites with site spacings of approximately 2-10 km (Figure 8). We used AMT data to constrain cover thickness as an aid to selecting drilling targets and to refine sedimentary basin extents. We also used broadband MT data to image deeper crustal architecture and to characterise the geometry of major structures. The broadband MT results will be presented in a separate paper.

We inverted AMT data at all 131 sites, using 32 Markov chains each sampling 1 million models. Figure 9 gives examples of inversion results at a few of the initially proposed National Drilling Initiative drill sites. Figure 10 shows spatially interpolated cover thickness from all the MT sites using the Inverse Distance Weighted method, along with a FWHM plot as a quantification of the uncertainty in the most likely interface change between the overlying sedimentary basins and the basement.

All the models show a conductive near-surface layer (<20 ohm.m) approximately 50 m thick, representing the weathered top of the Georgina Basin (Figure 9). Beneath is a moderately resistive layer (a few hundred ohm.m), suggesting a mixture of sedimentary rocks of the Georgina Basin and volcanic rocks (Helen Springs Group) of the Kalkarindji Igneous Province (Glass, 2002; Glass and Phillips, 2006). At greater depths (a few hundred metres), a transition to highly resistive basement occurs at some sites, mostly those to the southeast of the Gulunguru Fault, e.g., at site ET09n (Figure 9). At some sites to the northwest of the Gulunguru Fault, conductive materials are observed at depths of a few hundred to ~2000 m, possibly representing black shales within the basin sequences, i.e. the Mullera Formation of the South Nicholson Basin – sites ET02n and ET018 are two examples. The recessive Mullera Formation contains organic-rich shale and minor ironstone which contribute to enhanced conductivities. Its thickness is estimated to be greater than 1100 m in the Northern Territory (Carter and Zimmerman, 1960). Based on our results, we suggest that the Mullera Formation could be present at a depth of a few hundred metres and reach substantial thickness northwest of the Gulunguru Fault in the East Tennant region. Spatially interpolated cover thickness (Figure 10a) indicates that the Paleo- and Mesoproterozic basin sequence is fault bounded by the Gulunguru Fault, suggesting a thicker cover to the northwest and a thinner cover (a few hundred metres) comprising only the Georgina Basin and Kalkarindji Province to the southeast of the Gulunguru Fault.

In terms of uncertainty, as shown in Figure 9, the 80% credible interval (bounded by the dashed lines) is significantly higher in the more resistive parts of the model. This is expected because it is well known that MT responses are more sensitive to conductive material than

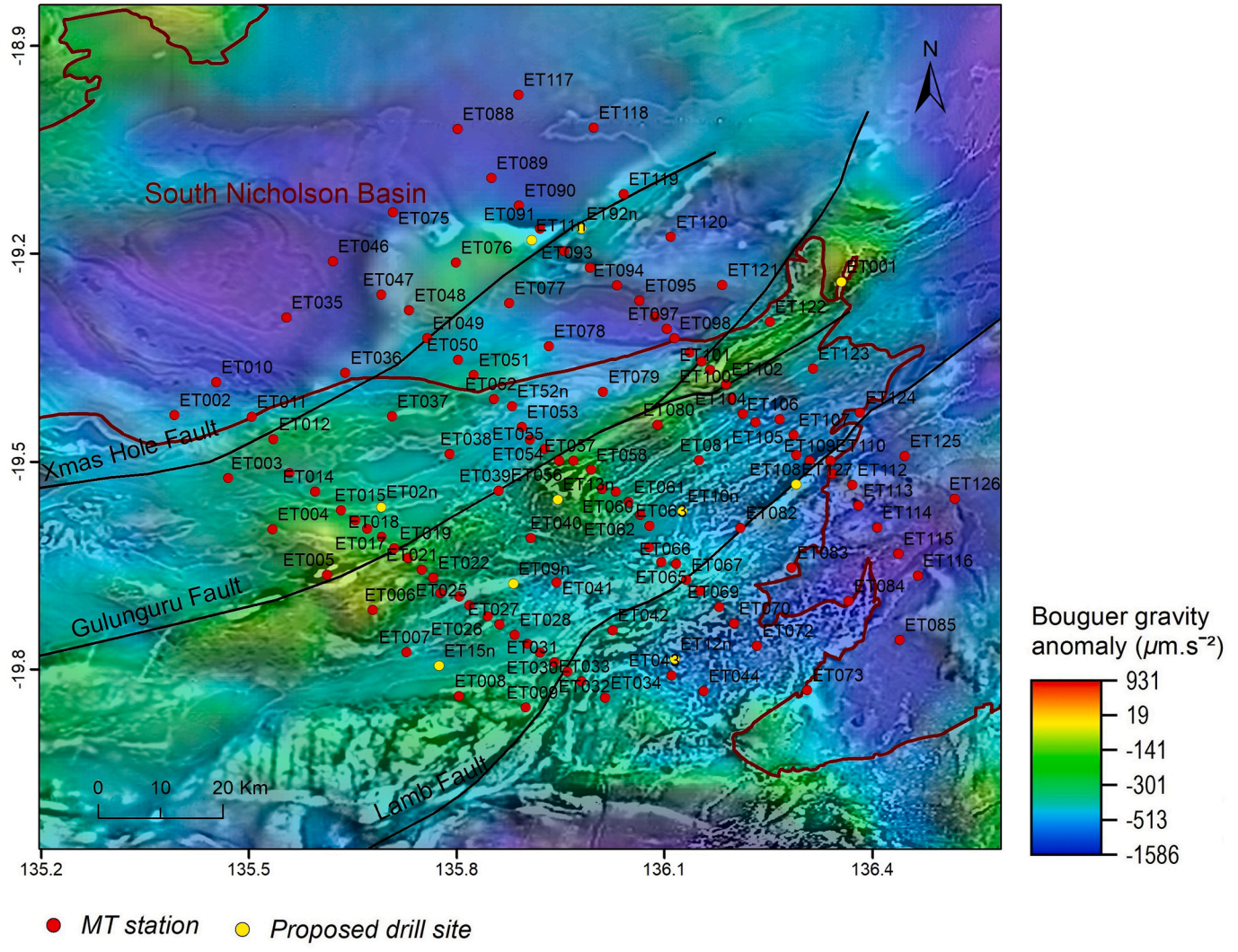

Fig. 8. Broadband and AMT stations in the East Tennant region. Black lines show the trace of major faults interpreted from seismic reflection and potential-field data (Clark et al., 2021). Brown lines mark the previously interpreted extent of the South Nicholson Basin based on sparse borehole and potential-field data. The background map is the Bouguer gravity anomaly map (Nakamura, 2016) overlain on the first vertical derivative of the reduced to pole magnetics map of Australia, 6th Edition (Nakamura and Milligan, 2015).

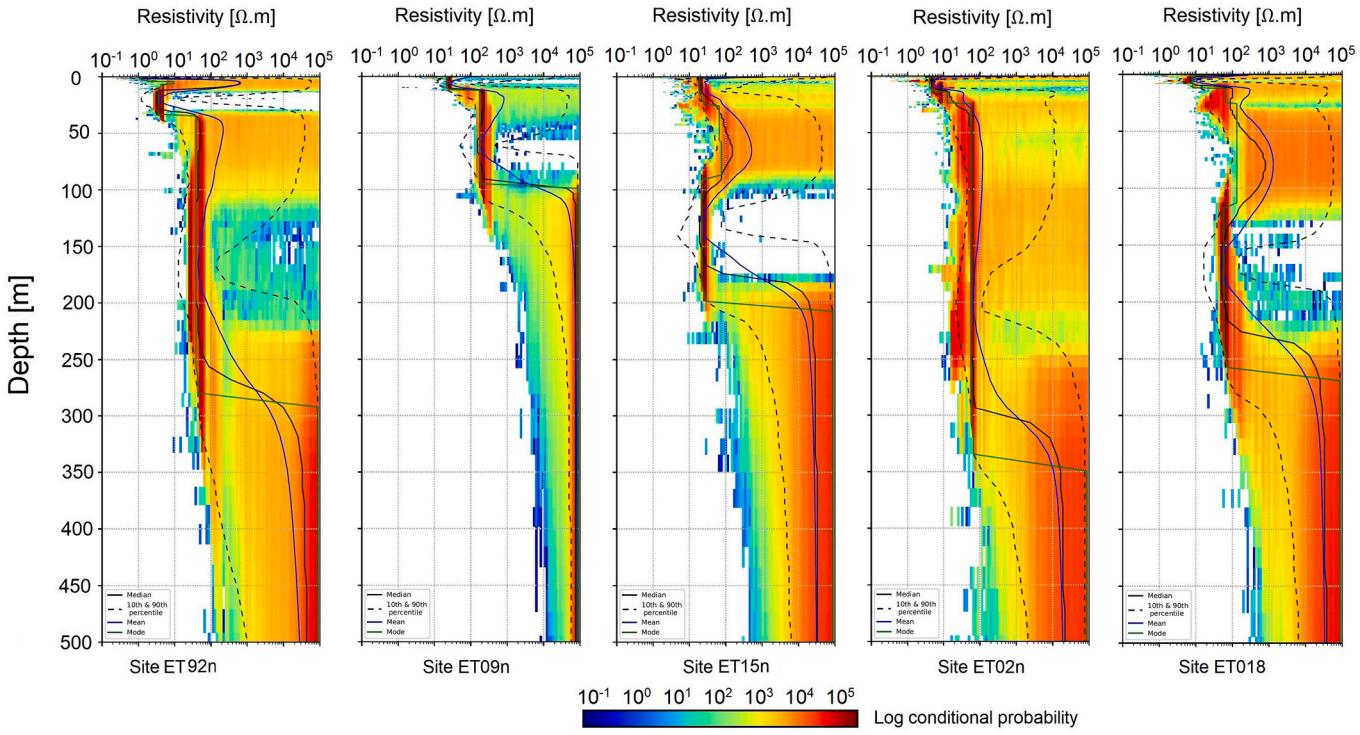

Fig. 9. Examples of the 1D probabilistic inversion results at a selection of proposed drill sites in the East Tennant region: the summary median, 10th and 90th percentile, mean and mode models overlie the pseudo-coloured shaded image of the 2D log-PPD histogram.

resistive material. In addition, Figure 10b shows that cover thickness estimates are generally more accurate at sites with thinner cover to the southeast of the Gulunguru Fault, with a few exceptions (e.g. ET046, ET038). Figure 11 indicates a moderately positive linear relationship between cover thickness estimates and uncertainty quantified by the FWHM, except at two outliers (ET010 and ET079). It is unsurprising that uncertainties in the cover thickness estimates increase with depth given that data sensitivity declines with depth. Sites with greater than ~600 m uncertainty (FWHM) represent sites with poorly defined peaks in the change-point histogram and uncertainty estimates using the FWHM may not be appropriate.

Cover thickness estimates at proposed drill sites have assisted with stratigraphic drill targeting. For example, the cover thickness estimate at ET92n (Fig. 9 and Fig. 10a) confirms a newly recognised basement high, which is at a drillable depth (borehole NDIBK06). At site ET015n, the model result suggests the basement is unlikely to be reached until 760 m. Therefore, this drill site was moved ~12 km northeast (NDIBK10). At site ET02n and a few surrounding sites, e.g. site ET018, the top of the basement is likely as deep as ~1000 m due to the presence of the South Nicolson Basin. Therefore, this site was not drilled. All the final drill sites were selected to the southeast of the Gulunguru Fault, except site NDIBK06.

In December 2020, the 10-hole, 4000 m drilling campaign was successfully completed in the East Tennant region as part of the National Drilling Initiative. We have validated the models against the drilling results to improve our geophysical interpretations. Fig. 12 shows a comparison between cover thickness estimates from the inversion models and those interpreted from drilling results. At sites ET10n, ET015 and ET008, significant resistivity increase occurred at the top of basement granitic rocks where cover thickness estimates compare favourably with drilling results with an accuracy of 0.7% - 5.4%. At the rest of the sites, where the Georgina Basin comprises a more siliciclastic-rich lower part, AMT couldn't discriminate those sedimentary rocks from the basement rocks. Therefore, the resistivity contrast marks the top of siliciclastic rocks above Helen Springs Volcanics, rather than the basement. For example, at NDIBK10, siliciclastic sedimentary basin infill is approximately 726 m deep. Greater discrepancy is observed at these sites. We will undertake a more rigorous analysis of these comparisons as interpretation of the drilling results progresses.

5. Discussion and conclusion

We have used trans-dimensional Bayesian inversion to solve for an ensemble of resistivity-depth models. The probabilistic method has a few advantages over deterministic inversion methods. First of all, it gives a thorough exploration of model space and a more robust estimation of uncertainty than deterministic methods allow. The inversion results are driven by data and relatively uninformed uniform priors; therefore, they are global and robust (Chen et al., 2012). The algorithm provides a wealth of information about unknown model parameters which allow for a reliable quantification of non-uniqueness and uncertainty. Second, the trans-dimensional aspect of the algorithm allows the number of layers in the resistivity model to be an unknown. This feature means users do not need to pre-select the model layer structure. This is especially appealing when inverting geophysical data collected in greenfield regions where prior knowledge of the geology may not be adequate and pre-selection of layers can bias results. Third, the method gives pronounced layer boundaries that allow more straightforward and repeatable interpretation of resistivity structures than is possible from regularised smooth model inversions. Last, the method is not subject to starting model sensitivity and instability issues that are sometimes encountered in gradient methods. The code is embarrassingly parallel and resources from the National Computational Infrastructure (NCI Australia) allow hundreds of sites to be inverted within hours.

Geophysical techniques are applicable to cover thickness estimation where they can detect physical property contrasts between cover sequences and basement rocks. For example, we have used MT data to image electrical conductivity contrast; refraction seismic to calculate distinct velocities corresponding to different stratigraphic units; and magnetic data to estimate depth to magnetic basement rocks given that

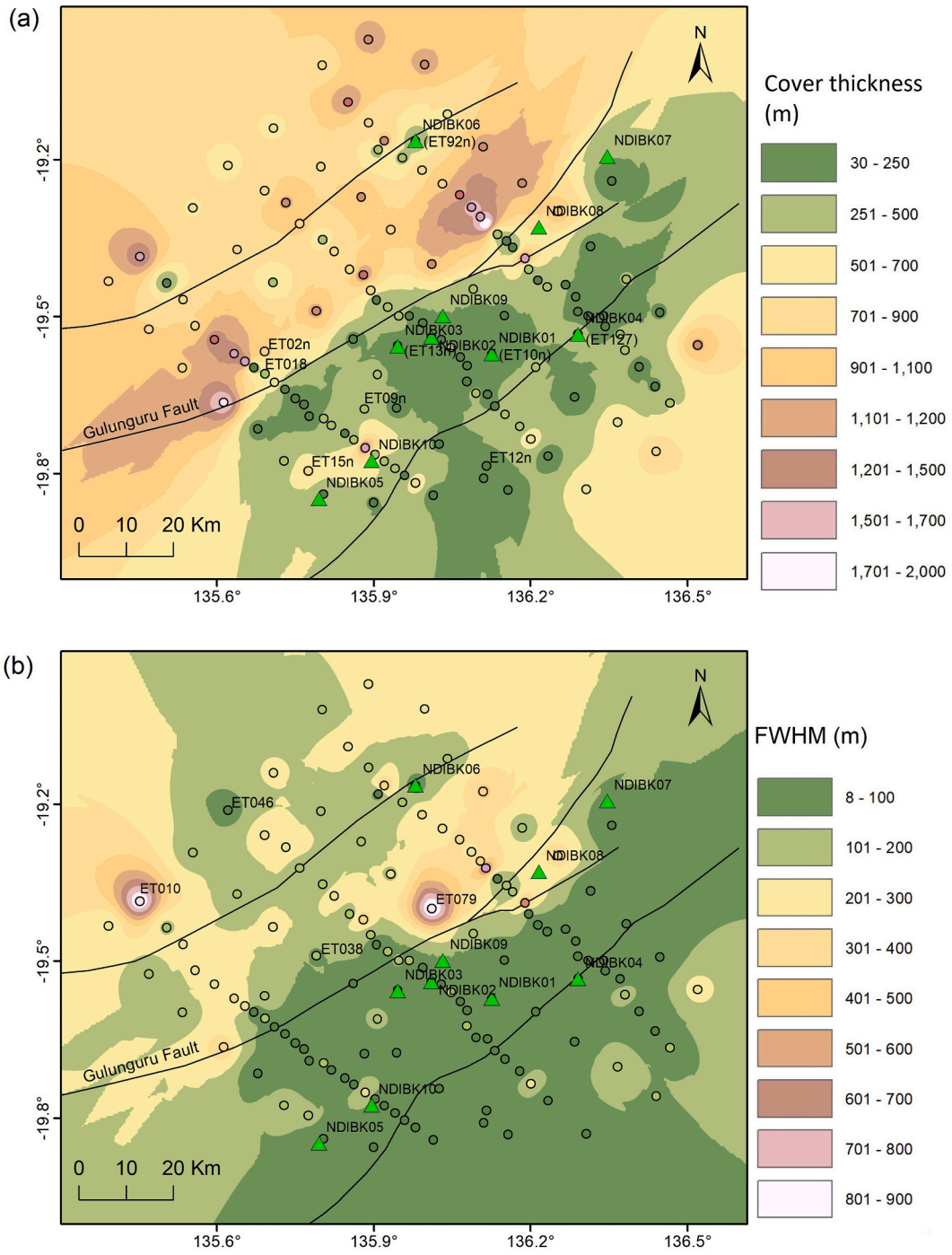

Fig. 10. (a) Cover thickness estimates from inversion of AMT data using the rj-McMCMT method in the East Tennant region; (b) FWHM uncertainty of the peak distribution for the mostly likely depth to basement. This spatially interpolated surface was generated using an Inverse Distance Weighted method. Green triangles show the final National Drilling Initiative drill sites, which in some cases differ from the initially proposed sites shown in Figure 8. Black lines show the trace of major faults interpreted from seismic reflection and potential-field data (Clark et al., 2021).

cover sequences are non-magnetic. Other researchers have successfully used passive seismic data to retrieve sedimentary basin geometry by applying Receiver Functions method (Piana Agostinetti et al., 2018), teleseismic P-wave delays method (Piana Agostinetti and Martini, 2019), and teleseismic auto-correlations (Phạm and Tkalčić, 2017). Each geophysical technique has capabilities and limitations, therefore, they are preferably used in conjunction to provide complementary information.

The application of the MT method to cover estimation has been validated and the results compare favourably with borehole stratigraphy logs. This demonstrates that the method is capable of identifying major stratigraphic structures with resistivity contrasts. Our results have assisted with the planning of regional drilling programs and have helped to reduce the uncertainty and risk associated with intersecting targeted stratigraphic units in covered terrains.

From an exploration perspective, mapping sedimentary basins and covered near-surface geological features supports the effective search for mineral deposits in the upper crust in greenfield areas. Interpretation of the AMT data has improved our understanding of the distribution and geometries of sedimentary basins; in some cases, their configurations

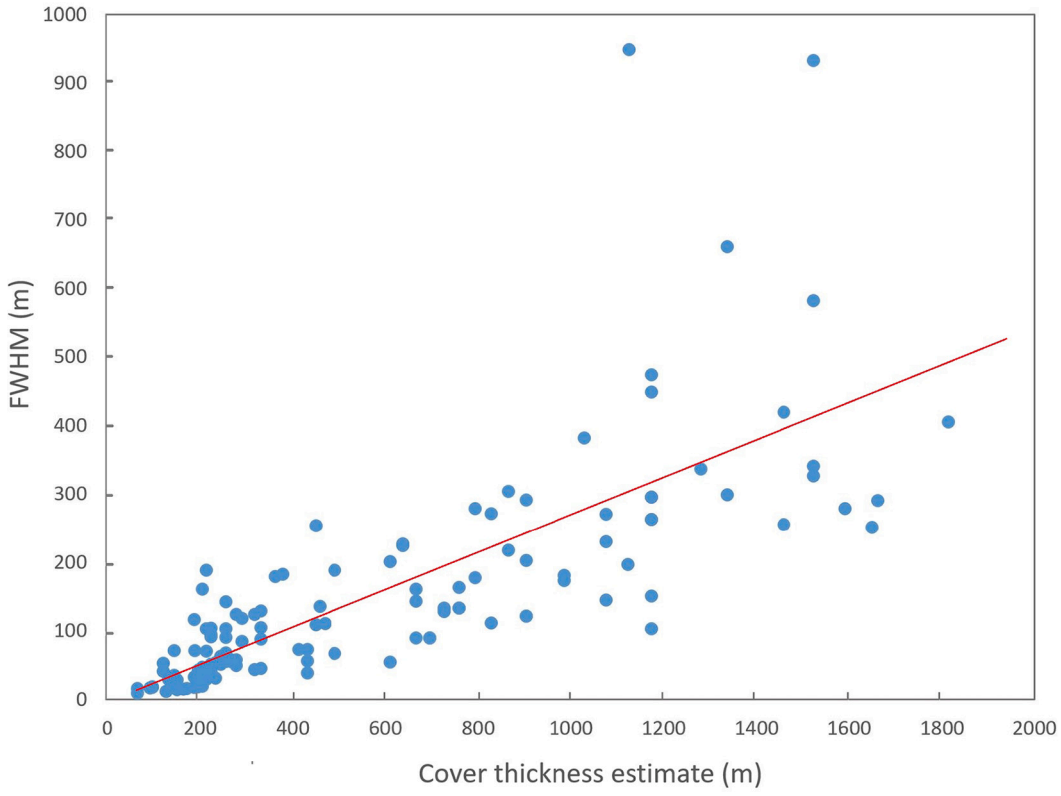

Fig. 11. Scatterplot showing correlation between cover thickness estimates and uncertainty quantified by FWHM for the 131 stations in the East Tennant region. The red trend line indicates a moderately positive linear relationship.

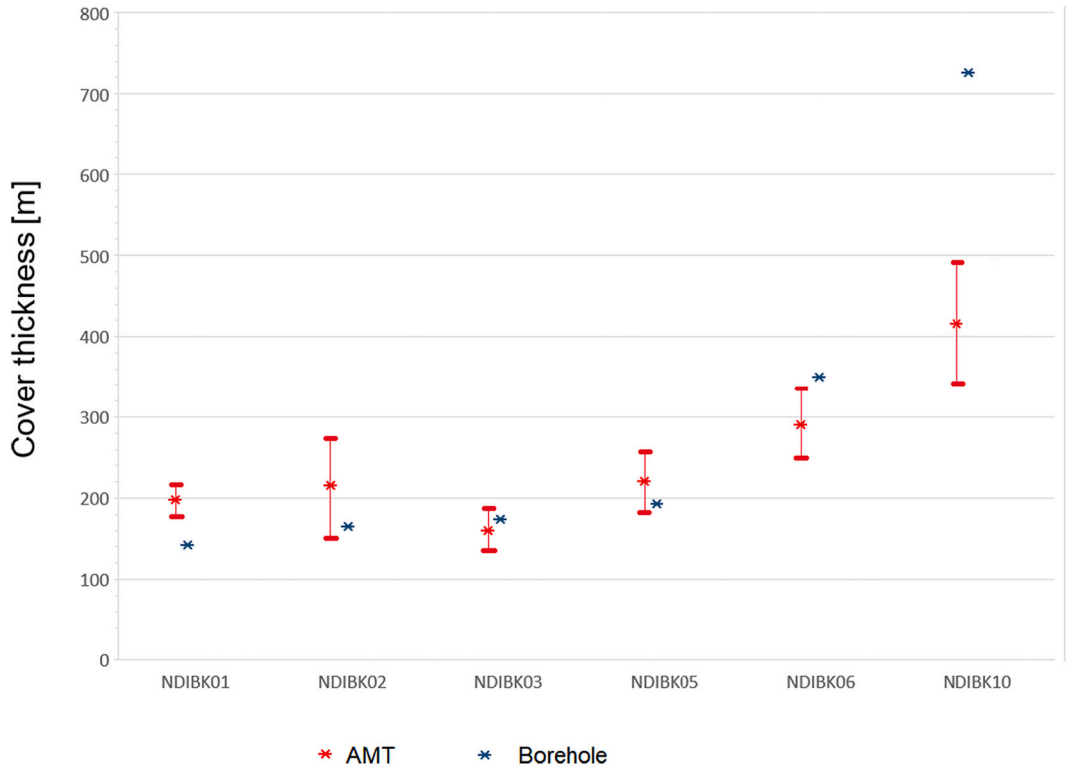

Fig. 12. Comparison of cover thickness estimates with uncertainty (FWHW) from the rjMcMCMT 1D inversion models with drilling results from the National Drilling Initiative campaign in the East Tennant region. Depths are true vertical depth in meters.

were previously interpreted based only on sparse borehole and potential-field data which are relatively insensitive to depth.

Code and data accessibility

The *rj-McMCMT* code is accessible as *C++* source code and as executables for 64-bit Windows® PCs. The source code is packaged in a Git repository and can be downloaded from Geoscience Australia's GitHub® repository https://github.com/GeoscienceAustralia/rjmcmcmt. The code can be compiled using most modern *C++* compilers on both Linux and Windows® based systems.

The source code and binaries are released under the GNU GPL Version 2.0 Licence, making it available for anyone to use at no cost, including for academic, government and commercial purposes. All of the programs are command line driven and hence do not have graphical user interfaces. The code is accompanied by basic user documentation and examples. However, Geoscience Australia will not be providing user support for the source code installation and/or program usage.

Data used in this paper have been publicly released by Geoscience Australia. MT data in the Southern Thomson (Jiang, 2017) can be accessed via http://pid.geoscience.gov.au/dataset/104240; MT data in the Coompana Province (Jiang et al., 2017) can be accessed via http://pid.geoscience.gov.au/dataset/112942; and MT data in the East Tennant region (Jiang and Duan, 2019) can be accessed via http://pid.geoscience.gov.au/dataset/ga/132016.

CRediT authorship contribution statement

Wenping Jiang: Conceptualization, Methodology, Software, Data curation, Visualization, Writing – original draft. **Ross C. Brodie:** Conceptualization, Methodology, Software, Writing – review & editing. **Jingming Duan:** Conceptualization, Methodology, Investigation, Writing – review & editing. **Ian Roach:** Investigation, Writing – review & editing. **Neil Symington:** Methodology, Writing – review & editing. **Anandaroop Ray:** Methodology, Writing – review & editing. **James Goodwin:** Visualization, Writing – review & editing.

Declaration of Competing Interest

The authors declare that they have no known competing financial interests or personal relationships that could have appeared to influence the work reported in this paper.

Data availability

I have provided code and data accessibility

Acknowledgments

We acknowledge all landholders and traditional custodians of the lands on which this work was undertaken; their cooperation and support allowed the data presented in this paper to be collected.

We thank Professor Malcolm Sambridge and Dr Rhys Hawkins from the Research School of Earth Sciences, Australian National University, for their advice on the method and assistance with their open-source rj-McMC library on iEarth.

Funding and support from Geoscience Australia's Exploring for the Future program, MinEx CRC, State and Northern Territory Geological Surveys made this publication possible.

We acknowledge constructive reviews and comments by the two reviewers. We also thank Adrian Hitchman and Josef Holzschuh for their valuble comments on an earlier version of this manuscript.

This paper is published with the permission of the CEO, Geoscience Australia.

References

Armistead, S.E., Skirrow, R.G., Fraser, G.L., Huston, D.L., Champion, D.C., 2017. Gold and intrusion-related Mo-W mineral systems of the southern Thomson Orogen, New South Wales. In: Record 2017/005. Geoscience Australia, Canberra. doi:10.11636/Record.2017.005.

Bayes, T., Price, R., 1763. An Essay towards Solving a Problem in the Doctrine of Chances. By the Late Rev. Mr. Bayes, F. R. S. Communicated by Mr. Price, in a Letter to John Canton, A. M. F. R. S. Philosophical Transactions (1683-1775), 53, pp. 370–418.

Blake, D.H., Kilgour, B., (Cartographer)., 2012. Geological Regions of Australia, 1:5 000 000 scale. Geoscience Australia, Canberra.

Blatter, D., Key, K., Ray, A., Gustafson, C., Evans, R., 2019. Bayesian joint inversion of controlled source electromagnetic and magnetotelluric data to image freshwater aquifer offshore New Jersey. Geophys. J. Int. 218 (3), 1822–1837.

Blatter, D., Ray, A., Key, K., 2021. Two-dimensional Bayesian inversion of magnetotelluric data using trans-dimensional Gaussian processes. Geophys. J. Int. 226 (1), 548–563.

Bodin, T., Sambridge, M., 2009. Seismic tomography with the reversible jump algorithm. Geophys. J. Int. 178 (3), 1411–1436.

Bodin, T., Sambridge, M., Gallagher, K., Rawlinson, N., 2012. Transdimensional inversion of receiver functions and surface wave dispersion. J. Geophys. Res. 117 (B2).

Booker, J.R., 2014. The Magnetotelluric Phase Tensor: A Critical Review. Surv. Geophys. 35 (1), 7–40.

Brodie, R.C., Jiang, W., 2018. Trans-dimensional monte carlo inversion of short period magnetotelluric data for cover thickness estimation. ASEG Extended Abstr. 2018 (1), 1–7.

Brodie, R.C., Sambridge, M., 2012. Transdimensional Monte Carlo Inversion of AEM Data. ASEG Extended Abstr. 2012 (1), 1–4.

Cagniard, L., 1953. Basic theory of the magnetotelluric method of geophysical prospecting. Geophysics 18, 605–635.

Caldwell, T.G., Bibby, H.M., Brown, C., 2004. The magnetotelluric phase tensor. Geophys. J. Int. 158 (2), 457–469.

Carter, E.K., Zimmerman, D.O., 1960. Constance range iron deposits, northwestern Queensland. In: B. o. M. Resources.

Chen, J., Hoversten, G.M., Key, K., Nordquist, G., Cumming, W., 2012. Stochastic inversion of magnetotelluric data using a sharp boundary parameterization and application to a geothermal site. Geophysics 77 (4), E265–E279.

Clark, A., Highet, L., Schofield, A., Doublier, M., 2021. Solid Geology map of the East Tennant region. In: Geoscience Australia, Canberra doi: http://pid.geoscience.gov.au/dataset/ga/145260.

Constable, S.C., Parker, R.L., Constable, C.G., 1987. Occam's inversion; a practical algorithm for generating smooth models from electromagnetic sounding data. Geophysics 52 (3), 289–300.

Czarnota, K., Hoggard, M.J., Richards, F.D., Teh, M., Huston, D.L., Jaques, A.L., Ghelichkhan, S., 2020. Minerals on the edge: Sediment-hosted base metal endowment above steps in lithospheric thickness. In: Geoscience Australia, Canberra. https://doi.org/10.11636/134991.

Denison, D.G.T., Holmes, C.C., Mallick, B.K., Smith, A.F.M., 2002. Bayesian Methods for Nonlinear Classification and Regression. Wiley, Chichester.

Dettmer, J., Dosso, S.E., 2013. Probabilistic two-dimensional water-column and seabed inversion with self-adapting parameterizations. J. Acoust. Soc. Am. 133 (5), 2612–2623.

Dmitriev, V.I., Berdichevsky, M.N., 1979. The fundamental model of magnetotelluric sounding. Proc. IEEE 67 (7), 1034–1044.

Dutch, R., Wise, T., Pawley, M., Tylkowski, L., Lockheed, A., Jagodzinski, L., Heath, P., 2017. PACE Copper Coompana Drilling Project_ Drillhole CDP003 preliminary field-data report.

Ferguson, I.J., Jones, A.G., Sheng, Y., Wu, X., Shiozaki, I., 1999. Geoelectric response and crustal electrical-conductivity structure of the Flin Flon Belt, Trans-Hudson Orogen, Canada. Can. J. Earth Sci. 36 (11), 1917–1938.

Gallagher, K., Bodin, T., Sambridge, M., Weiss, D., Kylander, M., Large, D., 2011. Inference of abrupt changes in noisy geochemical records using transdimensional changepoint models. Earth Planet. Sci. Lett. 311 (1), 182–194.

Glass, L.M., 2002. Petrogenesis and Geochronology of the north Australian Kalkarinji low-Ti Continental Flood Basalt Province (PhD thesis),. Research school of Earth Sciences, Australian National University, Canberra.

Glass, L.M., Phillips, D., 2006. The Kalkarindji Continental Flood Basalt Province. A new Cambrian Large Igneous Province in Australia with possible links to mass extinction. Geology 34 (6), 461–464.

Goodwin, J.A., Jiang, W., Meixner, A.J., McAlpine, S.R.B., Buckerfield, S., Nicoll, M.G., Crowe, M., 2017. Estimating Cover Thickness in the Southern Thomson Orogen - Results from the pre-drilling application of refraction seismic, audio-magnetotelluric and targeted magnetic inversion modelling methods on proposed borehole sites. In: Record 2017/021: Geoscience Australia, Canberra. https://doi.org/10.11636/Record.2017.021.

Goodwin, J.A., Roach, I.C., Meixner, T.J., Jiang, W., Holzschuh, J., Davies, L., 2018. Estimating Cover Thickness in the Southern Thomson Orogen – A Comparison of Applied Geophysics Estimates with Borehole Results. ASEG Extended Abstracts, 2018, 1(1-8).

Green, P.J., 1995. Reversible jump Markov chain Monte Carlo computation and Bayesian model determination. Biometrika 82, 711–732.

Hawkins, R., 2013. iEarth web page for rj-McMC. Retrieved from. http://www.iearth.org.au/codes/rj-MCMC.

Jiang, W., 2017. Southern Thomson Pre-drilling Audio-magnetotelluric data. In: Geoscience Australia, Canberra. https://doi.org/10.26186/5c64d52d54413.
Jiang, W., Duan, J., 2019. East Tennant magnetotelluric survey. Geoscience Australia, Canberra, Northern Territory, Australia. https://doi.org/10.26186/5df80d8615367.
Jiang, W., McAlpine, S., Duan, J., Dutch, R., Pawley, M., 2017. Coompana Predrill Magnetotelluric Data. In: Geoscience Australia, Canberra. https://doi.org/10.4225/25/5a26133e93f0e.
Kaufman, A.A., Keller, G.V., 1981. The Magnetotelluric Sounding Method, 15. Elsevier Scientific, Amsterdam.
MacKay, D.J.C., 2003. Information Theory, Inference and Learning Algorithms. Cambridge Univ. Press.
Malinverno, A., 2002. Parsimonious Bayesian Markov chain Monte Carlo inversion in a nonlinear geophysical problem. Geophys. J. Int. 151 (3), 675–688.
Mandolesi, E., Ogaya, X., Campanyà, J., Piana Agostinetti, N., 2018. A reversible-jump Markov chain Monte Carlo algorithm for 1D inversion of magnetotelluric data. Comput. Geosci. 113, 94–105.
Minsley, B.J., 2011. A trans-dimensional Bayesian Markov chain Monte Carlo algorithm for model assessment using frequency-domain electromagnetic data. Geophys. J. Int. 187 (1), 252–272.
Murr, J., Skirrow, R.G., Schofield, A., Goodwin, J., Coghlan, R.A., Highet, L., Czarnota, K., 2020. Tennant Creek – Mount Isa IOCG mineral potential assessment. In: Czarnota, K., et al. (Eds.), Exploring for the Future: Extended Abstracts, 1-4. Geoscience Australia, Canberra.
Nakamura, A., 2016. *Bouguer Gravity Anomaly Colour Composite Image of Onshore Australia 2016.* Record 101102. Geoscience Australia, Canberra.
Nakamura, A., Milligan, P.R., 2015. Total magnetic intensity anomaly map Australia. (6th Edition) Record 89596. Geoscience Australia, Canberra.
Newman, G.A., Alumbaugh, D.L., 2000. Three-dimensional magnetotelluric inversion using non-linear conjugate gradients. Geophys. J. Int. 140 (2), 410–424.
Peng, R., Han, B., Liu, Y., Hu, X., 2022. A Julia software package for transdimensional Bayesian inversion of electromagnetic data over horizontally stratified media. Geophysics F55–F66.
Phạm, T.-S., Tkalčić, H., 2017. On the feasibility and use of teleseismic P wave coda autocorrelation for mapping shallow seismic discontinuities. J. Geophys. Res. Solid Earth 122 (5), 3776–3791.
Piana Agostinetti, N., Martini, F., 2019. Sedimentary basins investigation using teleseismic P-wave time delays. Geophys. Prospect. 67 (6), 1676–1685.
Piana Agostinetti, N., Martini, F., Mongan, J., 2018. Sedimentary basin investigation using receiver function: an East African Rift case study. Geophys. J. Int. 215 (3), 2105–2113.
Pratt, R.G., Shin, C., Hick, G.J., 1998. Gauss–Newton and full Newton methods in frequency–space seismic waveform inversion. Geophys. J. Int. 133 (2), 341–362.
Ray, A., Key, K., 2012. Bayesian inversion of marine CSEM data with a trans-dimensional self parametrizing algorithm. Geophys. J. Int. 191 (3), 1135–1151.
Ray, A., Sekar, A., Hoversten, G.M., Albertin, U., 2016. Frequency domain full waveform elastic inversion of marine seismic data from the Alba field using a Bayesian trans-dimensional algorithm. Geophys. J. Int. 205 (2), 915–937.
Roach, I.C., Brodie, R.C., Costelloe, M.T., 2015. The Southern Thomson AEM Survey. Geoscience Australia, Canberra doi: http://pid.geoscience.gov.au/dataset/ga/82628.
Roach, I.C., Brown, D.D., Purdy, D.J., McPherson, A.A., Gopalakrishnan, S., Barton, T.J., Cant, R., 2017. GSQ Eulo 1 borehole completion record: Southern Thomson Project. In: Record 2017/007. Geoscience Australia, Canberra. https://doi.org/10.11636/Record.2017.007.
Rodi, W.L., Mackie, R.L., 2001. Nonlinear conjugate gradients algorithm for 2-D magnetotelluric inversion. Geophysics 66 (1), 174.
Rodi, W.L., Mackie, R.L., 2012. The inverse problem. In: Chave, A.D., Jones, A.G. (Eds.), The Magnetotelluric Method: Theory and Practice. Cambridge University Press, New York, pp. 347–414.
Rothery, E., 2013. A new intrusion-related gold field in the Thomson Fold Belt, NSW. In: Paper presented at the Proceedings of the Mines and Wines Conference. Maitland NSW: Geological Survey of NSW, Orange, NSW.
Roy, I.G., 2002. A robust descent type algorithm for geophysical inversion through adaptive regularization. Appl. Math. Model. 26 (5), 619–634.
Sambridge, M., Bodin, T., Gallagher, K., Tkalčić, H., 2013. Transdimensional inference in the geosciences. Phil. Trans. R. Soc. A 371, 20110547.
Schofield, A., Clark, A., Doublier, M.P., Murr, J., Skirrow, R.G., Goodwin, J.A., Roach, I. C., 2020. Data integration for greenfields exploration: an example from the East Tennant region, Northern Territory. In: Czarnota, K., et al. (Eds.), Exploring for the Future: Extended Abstracts, 1-4. Geoscience Australia, Canberra.
Siripunvaraporn, W., Egbert, G., 2007. Data space conjugate gradient inversion for 2-D magnetotelluric data. Geophys. J. Int. 170 (3), 986–994.
Skirrow, R.G., Murr, J., Schofield, A., Huston, D.L., van der Wielen, S., Czarnota, K., Duan, J., 2019. Mapping iron oxide Cu-Au (IOCG) mineral potential in Australia using a knowledge-driven mineral systems-based approach. Ore Geol. Rev. 113, 103011.
Szarka, L., Menvielle, M., 1997. Analysis of rotational invariants of the magnetotelluric impedance tensor. Geophys. J. Int. 129, 133.
Tikhonov, A.N., 1950. The determination of the electrical properties of deep layers of the earth's crust. Dokl Acad Nauk SS (73), 295–297.
Vozoff, K., 1991. The magnetotelluric method. In: M, N. (Ed.), Electromagnetic methods in applied geophysics II. Society of Exploration Geophysicists, Tulsa Oklahoma.
Ward, S.H., Hohmann, G.W., 1988. Electromagnetic Theory for Geophysical Applications. In: Electromagnetic Methods in Applied Geophysics: Volume 1, Theory, pp. 130–311.
Xiang, E., Guo, R., Dosso, S.E., Liu, J., Dong, H., Ren, Z., 2018. Efficient hierarchical trans-dimensional Bayesian inversion of magnetotelluric data. Geophys. J. Int. 213 (3), 1751–1767.